Received: 28 January 2024 | Accepted: 5 May 2024

DOI: 10.1002/vzj2.20350

Vadose Zone Journal

ORIGINAL ARTICLE

Special Section: Tribute to Rien van Genuchten, Recipient of the 2023 Wolf Prize for Agriculture

Pore unit cell network modeling of the thermal conductivity dynamics in unsaturated sandy soils: Unveiling the role of spanning-wetting phase cluster

Rasoul Mirghafari[1] | **Amir Hossein Helforoosh**[2] | **Ehsan Nikooee**[2] | **Ghassem Habibagahi**[2] | **Amir Raoof**[3] | **Martinus Theodorus van Genuchten**[3,4]

[1]School of Engineering, Computing and Mathematics, Oxford Brookes University, Oxford, UK

[2]Department of Civil and Environmental Engineering, Shiraz University, Shiraz, Iran

[3]Department of Earth Sciences, Utrecht University, Utrecht, The Netherlands

[4]Department of Nuclear Engineering, Federal University of Rio de Janeiro, UFRJ, Rio de Janeiro, Brazil

Correspondence
Ehsan Nikooee, Department of Civil and Environmental Engineering, Shiraz University, P.O. Box: 71348-51156, Shiraz, Iran.
Email: enikooee@shirazu.ac.ir

Assigned to Associate Editor Jan Hopmans.

Abstract

As the world struggles with climate change and energy crises, understanding the role of soil in the food–water–energy nexus becomes increasingly critical. Accurately estimating the soil thermal conductivity drying curve is essential for assessing the impacts of temperature on soil biota and crop growth, environmental changes due to forest fires and global warming, and for designing geo-energy extraction techniques such as geothermal energy piles. Existing empirical models often fail to accurately estimate the soil thermal conductivity (TC), particularly in pendular soil moisture regimes where they do not capture sharp changes in TC. This study introduces a novel approach using a pore unit cell network model to more accurately describe the dynamics of TC in variably saturated soils. A quadratic parallel scheme within each soil pore unit cell links the TCs of solid, water, and air to the overall effective conductivity. By modeling air invasion in the pore network model and employing the proposed equation, we determined the unsaturated soil TC based on varying local conductivities. The model effectively captures the significant decrease in conductivity in the pendular saturation regime, associated with the shrinkage of the spanning-wetting cluster. Quantitative analyses showed a substantial improvement in prediction accuracy compared to existing models, especially under varying moisture conditions. Our findings have significant implications for better characterizing soil thermal and hydraulic properties, which are crucial for resource management in a changing climate and advancing geo-energy technologies.

Abbreviations: GA, genetic algorithm; MAPE, mean absolute percentage error; NMR, nuclear magnetic resonance; PNM, pore network model; PUCNM, pore unit cell network model; RMSE, root mean squared error; SWRC, soil–water retention curve; TC, thermal conductivity; TCDC, soil thermal conductivity drying curve.

1 | INTRODUCTION

The global population is projected to exceed 9 billion by 2050 and approach 10.4 billion by the mid-2080s (McKersie, 2015; UN, 2023). With this growth, the demand for energy, water, and food will intensify, underscoring the need for more efficient management of our natural resources. Precise modeling of the water–food–energy nexus is vital for optimal resource utilization and adapting to rapidly changing climate conditions. A critical component of applicable models is accurate simulation of soil heat and water transport to allow more precise studies of the interplay between the anthroposphere, hydrosphere, and atmosphere.

Soil thermal properties are essential to accurately modeling heat transfer processes in soils. They are important for devising appropriate irrigation models for different soils (Zhang et al., 2019), managing soil moisture in general (Sanuade et al., 2020), estimating soil surface evaporation, assessing organic matter decomposition (Khaledi et al., 2023), and enhancing crop growth (Abu-Hamdeh, 2000; Abu-Hamdeh & Reeder, 2000). They are increasingly important also for designing energy-efficient building systems and geothermal piles (Akrouch et al., 2016; Bayat et al., 2021; Moradshahi et al., 2021). As climate change influences the frequency of forest fires (Flannigan et al., 2000), accurate models of soil heat transfer are critical to predict soil temperature variations, temperature-induced changes in soil quality (e.g., organic matter content), and carbon transfer to the atmosphere (Caon et al., 2014; Conant et al., 2011; Qi et al., 2016).

The importance of accurately estimating soil thermal properties is highlighted in numerous applications in the environmental and soil sciences, geoengineering, and atmospheric sciences. Examples include soil temperature variations and their effects on soil biota and plant growth (Heinze et al., 2017), understanding frost progression in cold regions (Hayashi et al., 2007), designing buried pipelines and pipeline thermal backfills (Jia et al., 2019; Newson & Brunning, 2004; Patwa et al., 2022), backfilling buried high-voltage power cables (Ocłoń, 2021), and developing bridge deck de-icing systems (Lei et al., 2020; Yu et al., 2016), among other applications. In coarse-grained soils, heat conduction is the predominant mechanism of soil heat transfer, making the estimation of soil thermal conductivity (TC) essential for these types of applications. Soils are multiphase systems involving the air, water, and solid phases, each having significantly different TCs: ranging from 1.0 to 9.0 W m^{-1} K^{-1} for soil grains depending on mineral type, 0.6 W m^{-1} K^{-1} for water, and 0.025 W m^{-1} K^{-1} for air (Côté & Konrad, 2005; Farouki, 1981; Johansen, 1977, among others). The multiphase nature of soils deems it necessary to obtain estimates of the overall effective soil TC, denoted hereafter by λ. The TC hence depends on many factors such as soil mineralogy, pore structure, bulk density, and the inherently transient nature of the soil moisture regime (Gamage et al., 2019; He et al., 2021; Lehmann et al., 2003; Mustamo et al., 2019; Zhao & Si, 2019). Furthermore, recent climate changes have led to new atmospheric and hydrological conditions, characterized by short bursts of intense rainfall and longer drought periods (Hirabayashi et al., 2008). These changing conditions underscore the importance of accurately characterizing soil thermal and hydraulic properties and their interplay, crucial for applications such as managing earth dams in extreme weather (Vahedifard et al., 2015). In this context, different effective TCs are expected due to changing moisture contents for the same soil type as a consequence of varying conditions of intense rainfall and drought.

Core Ideas

- Spanning-wetting cluster shrinkage in the pendular regime significantly decreases soil thermal conductivity.
- Soil thermal conductivity is influenced by both the distribution and specific values of local pore saturation.
- Pore unit cell network modeling leads to more accurate estimates of the unsaturated thermal conductivity.

The relationship between the soil thermal conductivity, hereafter denoted by λ, and the soil moisture content is often encapsulated in what is known as the soil thermal conductivity drying curve (TCDC). Various empirical or quasi-empirical equations for TCDC have been proposed to date (Campbell et al., 1994; Côté & Konrad, 2005; Hu et al., 2001; Likos, 2014a; Lu et al., 2007; Somerton et al., 1974). Recently, shifts have occurred toward the use of pore-scale models in attempts to obtain more precise predictions of the soil hydraulic and thermal properties. For example, Likos (2014b) utilized a unit pore model to determine the thermal conductivity for different pores based on the bundle of capillary tubes concept, along with a homogenization technique for upscaling, to find the TCDC. Although this model marks a significant advancement in physically based modeling of the TCDC, it has yet to fully address different features pertinent to soil pore structures made up of an assemblage of pore bodies and pore throats (Daneshian et al., 2021; Khaksar et al., 2013; Nikooee et al., 2014). For a more realistic representation of pore-scale soil moisture distributions, and consequently, accurate fluid saturation estimates at each matric suction, a model integrating both pore body and pore throat elements is essential. While drying processes are governed mostly by pore throat radii, they generally have minimal volume compared to pore bodies.

In this study, a pore network model (PNM) that accounts for various topological and geometrical characteristics of the soil pore structure is employed to determine the TCDC. The model effectively estimates soil moisture contents and distributions, thus providing a direct link between the soil water retention curve (SWRC) and the TCDC. It also elucidates how the evolution of continuous water clusters (or alternatively discontinuous water paths, and isolated pores) leads to three distinct saturation regimes with concomitant variations in the soil TC with saturation. We first present a brief review of previously proposed equations for the TCDC and their limitations. The proposed pore scale algorithm is then described in detail. Calculated TCDCs and SWRCs are subsequently compared against experimental data as well as the various TCDC equations. The discussion section explores the application scope of the method, while the study concludes with key insights, findings, and its future outlook.

2 | PREVIOUSLY PROPOSED EQUATIONS FOR THE TCDC

Most existing models for λ are based on the concept of a normalized thermal conductivity, as first introduced by Johansen (1977). These models interpolate λ between fully saturated and fully dry states of the soil medium, hereafter designated by λ_{sat} and λ_{dry}, respectively. A general expression for λ is given as:

$$\lambda(S) = f(S)(\lambda_{sat} - \lambda_{dry}) + \lambda_{dry}, \quad (1)$$

where $f(S)$ is a function of fluid saturation, S. The simplest forms for $f(S)$ include saturation or its square root (Somerton et al., 1974) as follows:

$$\lambda(S) = \sqrt{S}(\lambda_{sat} - \lambda_{dry}) + \lambda_{dry}, \quad (2)$$

Johansen (1975, 1977) suggested a logarithmic function for $f(S)$:

$$f(S) = 0.7\log(S) + 1 \ \text{ medium and fine sands}, \quad (3)$$

$$f(S) = \log(S) + 1 \ \text{ fine - textured soils}. \quad (4)$$

Côté and Konrad (2005) proposed another relationship based on the Kersten (1949) number, K_e, after analyzing a large database consisting of various soil types, including unfrozen and frozen gravels, sands, silts, clays, peat, and crushed rocks. The Kersten number is defined as:

$$f(S) = K_e = \frac{\kappa S}{1 + (\kappa - 1)S}, \quad (5)$$

where κ is a dimensionless parameter that varies with material type, with a recommended value of 3.55 for fine sands.

Another form of $f(S)$ based on heat pulse measurements involving a dozen sandy/silty soils was developed by Lu et al. (2007):

$$f(S) = \exp[\alpha(1 - S^{\alpha - 1.33})], \quad (6)$$

where α is a material parameter dependent upon soil type, with distinct values for coarse- and fine-grained soils, that is, 0.96 and 0.27, respectively (Dong et al., 2015; Likos, 2014b). Hu et al. (2001) furthermore used a log-linear function given by:

$$f(S) = [0.9879 + 0.181\ln(S)]. \quad (7)$$

Another commonly used physically based model for the thermal conductivity that accommodates various pore geometries and connections was proposed by de Vries (1963). His model considers the effective thermal conductivity of a partially saturated porous medium as the weighted sum of the thermal conductivities of water, air, and solid phases (Ghanbarian & Daigle, 2016; Hopmans & Dane, 1986a; Tarnawski et al., 2021). Subsequently, Campbell et al. (1994) modified the de Vries (1963) model by formulating the weight function for the conductivities of the endmembers (i.e., solid, water, and air) as continuous functions of saturation.

All of the above models attempt to relate bulk saturation to λ. However, as illustrated in Figure 1, the TCDC generally exhibits three distinct regions. A notable feature is the sharp decrease in λ that begins at around 20% saturation, marking the onset of the pendular regime where the liquid phase tends to become discontinuous (Fu et al., 2024; Likos, 2014b). This results in a two-part trend in the TCDC within this region. Unfortunately, the above equations do not adequately capture this phenomenon, which is likely influenced by pore-scale physics and the distribution of water between soil grains. We hypothesize, examined with the PNM, that increasing soil suctions and the resulting air invasion reduce the extent and number of water flow paths connecting the air and water reservoirs in the PNM. We anticipate that primarily mobile water and water within connected paths contribute to λ. In contrast, trapped water in pores surrounded by air-filled pores is presumed to conduct heat close to dry pores since their contribution is obscured by surrounding air-filled pores or pore clusters.

To the best of our knowledge, the thermal conductivity of unsaturated soils has not yet been explored from a pore scale network modeling perspective (i.e., incorporating a network composed of both pore body and pore throat elements). This study aims to correlate pore-scale saturation with the thermal conductivity of a single pore, then to upscale results in order to obtain the effective medium λ using the PNM. The

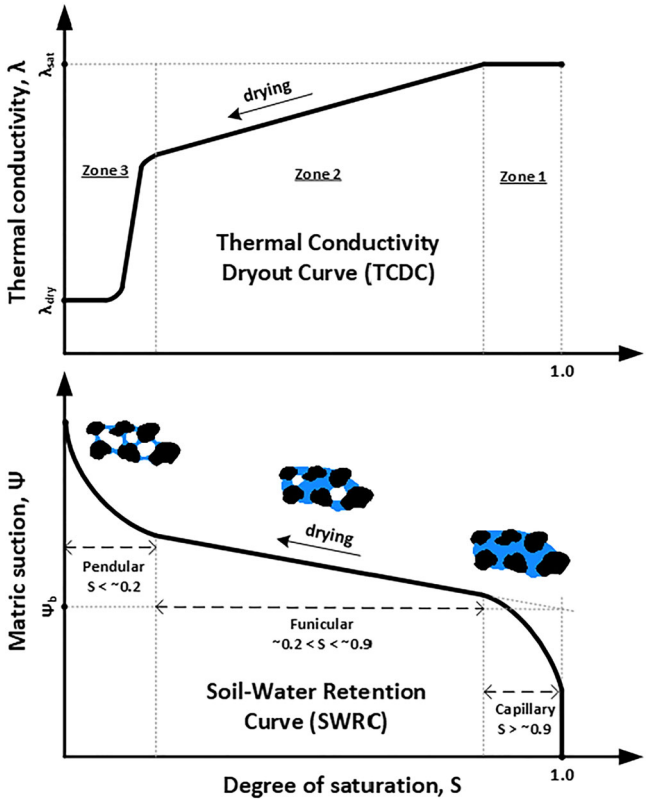

FIGURE 1 Schematics of the TCDC and the SWRC for a typical sand, depicting the relationships between soil saturation (S), matric suction, and the thermal conductivity, λ. The top schematic, based on Likos (2014b), showcases the significant changes in λ as the soil transitions through different saturation regimes, emphasizing the sharp decrease when entering the pendular regime.

approach involves pore-scale modeling of air invasion into a water-saturated network and determining λ with the PNM at each saturation level. With a pore skeleton that accurately captures the drying process of the PNM, this method is expected to yield more accurate TCDC estimations. Additionally, we investigate the impact of pore-scale characteristics such as coordination number and pore body and pore throat structural/mathematical parameters on the TCDCs. The database of sandy soils used in this study and the PNM approach are detailed in the following sections.

3 | MATERIALS AND METHODS

3.1 | Database of hydraulic and thermal properties of sandy soils

For this study, we compiled a database of measured values of the drying branch of the SWRCs and TCDCs of eight sandy soils. These soils are primarily classified as silty sand (SM) and poorly-graded sand (SP) according to the Unified Soil Classification System (ASTM, 1985). The data were sourced from studies by Likos (2014a, 2014b), Yao (2014), and Oh (2014). Table 1 presents the index soil properties and physical characteristics of the selected soils.

3.2 | PNM construction and computational method

A PNM was used next to simulate the SWRCs and TCDCs. The PNM along with its structural parameters was calibrated using a genetic algorithm (GA). We note that the calibration process only used measured SWRC data, with which we subsequently simulated the TCDCs. Our aim during calibration hence was to achieve the best possible match between the PNM simulations and the measured drying SWRC data. The simulations involved the following steps:

1. Generation of the PNM using initial estimates of the structural parameters.
2. Optimization of the structural parameters using SWRC experimental data in conjunction with GA.
3. Simulation of the drying processes.
4. Calculation of the unsaturated TCDC.

3.2.1 | The PNM generation algorithm

For this study, we used a regular PNM representing the pore structure of the sands. The network was modeled as a three-dimensional cubic lattice, where cubic pore bodies at the nodes are interconnected by cylindrical throats. The dimension of the PNM was determined by evaluating errors in predictions of the measured λ values (Figure 2). Formulations of the mean absolute percentage error (MAPE) and root mean squared error (RMSE) performance criteria provided in this figure are introduced in Table 2. A network comprising $40 \times 40 \times 40$ pores proved sufficient for capturing the experimental λ data and providing a representative elementary volume.

The simulated PNM was considered connected to a wetting phase (i.e., water) reservoir at the bottom and a non-wetting fluid (i.e., air phase) reservoir at the top. No-flow conditions were imposed along the lateral boundaries. A log-normal distribution function, consistent with previous studies (Daneshian et al., 2021; Raoof & Hassanizadeh, 2012; Rostami et al., 2015), was employed to generate pore body radii described by the following equation:

$$f(x|\mu,\sigma) = \frac{1}{x\sigma\sqrt{2\pi}} \exp\left(-\frac{(\ln(x)-\mu)^2}{2\sigma^2}\right), \quad (8)$$

where x denotes pore radii and μ and σ represent the mean and standard deviation of the lognormal distribution, respectively.

To determine the relationship between neighboring pores and their throat radius, the Acharya et al. (2004) formulas were used as illustrated in Figure 3 and expressed by

TABLE 1 Summary of index (physical) and thermal properties of the eight sandy soils considered in this study.

Soil name	n_p	G_s	D_{50} (mm)	C_u	C_c	$\lambda_{dry}(W/m\times K)$	$\lambda_{sat}(W/m\times K)$	Soil type	Reference
F-75 Sand	0.41	2.65	0.20	2.32	1.08	0.23	2.42	SP	Likos (2014b)
12/20 Sand	0.31	2.65	1.04	1.33	1.00	0.31	2.97	SP	Likos (2014b)
River sand	0.38	2.64	0.33	1.40	0.96	0.32	2.29	SP	Likos (2014a)
SM1	0.39	2.68	0.11	2.55	1.12	0.48	2.20	SM	Yao (2014)
SM2	0.40	2.75	0.13	3.20	1.01	0.38	2.17	SM	Yao (2014)
SP	0.37	2.66	0.21	1.60	1.03	0.40	2.43	SP	Oh (2014)
SP2	0.39	2.68	0.29	1.83	0.94	0.50	2.43	SP	Yao (2014)
SP5	0.37	2.66	0.21	1.59	1.03	0.40	2.43	SP	Yao (2014)

Abbreviations: n_p: soil porosity, G_s: specific gravity, D_{50}: median grain size (D_x, grain size at x % passing), C_u: uniformity coefficient (D_{60}/D_{10}), C_c: coefficient of curvature ($D_{30}^2/D_{60}\times D_{10}$), SM: silty sand, SP: poorly-graded sand.

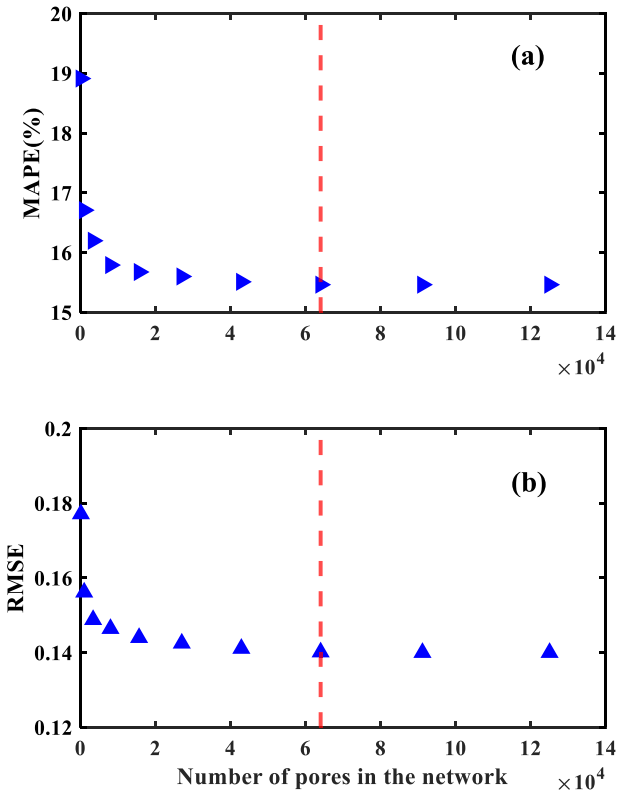

FIGURE 2 Variations in the (a) mean absolute percentage error (MAPE) and (b) root mean squared error (RMSE) performance measures of the unsaturated soil thermal conductivity drying curve (TCDC) of River sand versus size of the network (i.e., the number of pores in the pore network model [PNM]). The red line depicts 64,000 pores ($40\times40\times40$ pores).

Equation (9):

$$
\begin{aligned}
r'_{ij} &= p_i p_j \left(p_i^{(1/n)} + p_j^{(1/n)}\right)^{(-n)} \\
p_i &= \frac{R'_i \sin(\pi/4)}{(1-R'_i\cos(\pi/4))^n} \\
p_j &= \frac{R'_j \sin(\pi/4)}{(1-R'_j\cos(\pi/4))^n} \\
n>0, R'_i &= R_i/d_{ij}, R'_j = R_j/d_{ij}, r'_{ij} = r_{ij}/d_{ij}
\end{aligned}
\tag{9}
$$

TABLE 2 Measures of performance used in this study.

Error functions	Equations
Root mean squared error (RMSE)	$\text{RMSE} = \sqrt{\frac{1}{N}\sum_{i=1}^{N}(\lambda_{exp}-\lambda_{com})^2}$
Mean absolute percentage error (MAPE)	$\text{MAPE} = \frac{1}{N}\sum_{i=1}^{N}\frac{\lvert\lambda_{exp}-\lambda_{com}\rvert}{\lambda_{exp}}$
Coefficient of determination (R^2)	$R^2 = 1-\frac{\sum(\lambda_{exp}-\lambda_{com})^2}{\sum(\lambda_{exp}-\bar{\lambda})^2}$

Note: λ_{exp} and λ_{com} denote experimental and computed values of thermal conductivity data, respectively, and $\bar{\lambda}$ specifies the average value of the observed datapoints.

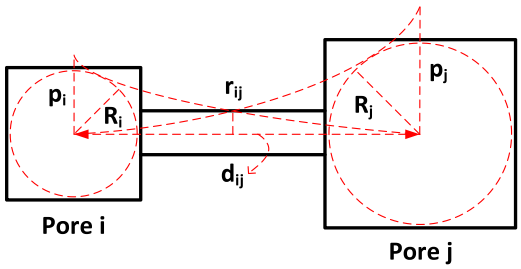

FIGURE 3 Schematic of a pore-to-pore connection within the pore network model (PNM), illustrating the geometric and topological setup of the cubic pore bodies and cylindrical pore throats.

where R_i and R_j are the radii of two adjacent pore bodies and r_{ij} is the radius of the cylindrical throat connecting them. The p_i and p_j values denote the distance between the center of pores i and j and the respective end of the arc tangent to the pore body and intersecting the pore throat (see Acharya et al. [2004] for further details). The distance between the pore body centers is denoted by d_{ij}, and n is a non-dimensional aspect ratio parameter governing the pore throat radius.

The coordination number C_n, representing the maximum and minimum number of neighboring pores, to which a pore can connect, varied between 6 and 2. In this study, the coordination number for various pores is controlled by the coordination number parameter, c, which ranges from 0 to 1.

This parameter acts as a threshold: a random number assigned to each throat determines if the throat is retained or removed based on its comparison to the parameter c. Thus, c influences the coordination number distribution. Consequently, the structural PNM parameters include the aspect ratio parameter (n), the coordination number parameter (c), the mean (μ) and standard deviation (σ) of the pore radii distribution, and the minimum ($R_{\min}$) and maximum ($R_{\max}$) pore body radii.

3.2.2 | PNM simulation processes

Simulation of SWRC and calibration of network structural parameters

The simulation process begins with an initial guess of the structural parameters, leading to the generation of a preliminary PNM. To accurately describe the soil's pore structure, a calibration and optimization technique is applied. The approach involves using the main drying branch of the SWRC experimental data for calibration. The structural parameters are iteratively modified until the error in predictions of the SWRC data falls below a predefined threshold. The GA is then employed to optimize the structural characteristics, ensuring that the simulated PNM closely aligns with the SWRC data.

The SWRC main drying branch is simulated as follows:

1. Generation of an initial PNM using assumed structural parameters and setting the top, bottom, and lateral boundary conditions.
2. Invasion of the non-wetting (air) phase into pores adjacent to the top boundary connected to the air reservoir. An air pressure is imposed along the top of the boundary of the pore network, while the bottom boundary is connected to the wetting phase reservoir. By stepwise increasing the air pressure, incremental matric suctions are applied to facilitate air invasion while maintaining a continuous drainage path. A pore is drained when air invades its connecting throat. The criterion for air invasion into a throat is defined by the Young–Laplace equation, which calculates the air entrance pressure for each throat during drainage:

$$P_{c_{\text{throat}}} = \frac{2T_s \cos\theta}{r_{ij}}, \tag{10}$$

where r_{ij} denotes the throat radius linking pores i and j, T_s represents surface tension, and θ specifies the receding contact angle.

3. Calculation of the degree of PNM saturation at each suction level (ψ) by identifying drained pores. Local saturation S_i of each cubic pore body i at different suction values is determined using a function proposed by Joekar-Niasar et al. (2010) in which R_i stands for the pore body radius:

$$S_i = -\frac{1}{6.83}\ln\left(1 - \frac{2T_s}{\psi R_i}\right). \tag{11}$$

4. Comparison of simulated and experimental SWRCs for a set of PNM structural parameters. The performance of the network is evaluated using the MAPE performance criterion:

$$\begin{aligned}\text{MAPE} &= f(n, c, \mu, \sigma, R_{\min}, R_{\max}) \\ &= \frac{1}{N}\sum_{i=1}^{N}\frac{\left|S_{\text{exp}} - S_{\text{pnm}}\right|}{S_{\text{exp}}},\end{aligned} \tag{12}$$

where S_{exp} and S_{pnm} are the experimental and simulated degrees of saturation, respectively, and N is the number of data points (suction levels).

5. Adjustment of structural parameters via GA, continuing until the error between experimental and simulated SWRCs is minimized, or a maximum number of algorithm generations is reached. The optimized structural parameters are then used to create the presumably most representative PNM.

Determination of TCDC

The thermal conductivity (λ) of each pore unit within the PNM is calculated using a quadratic parallel expression that combines the λ values of the solid, air, and water phases. The equation for calculating the λ of each soil unit embracing a pore is as follows (detailed calculations are provided in Appendix A):

$$\lambda(S) = \left[\frac{\kappa S}{1 + (\kappa - 1)S}\right](\lambda_{\text{sat}} - \lambda_{\text{dry}}) + \lambda_{\text{dry}}, \quad \kappa = 13, \tag{13}$$

where S denotes the local saturation of the pore, while the parameter κ is a function of soil structure, and the value obtained ($\kappa = 13$) is therefore suggested for sandy soils. The average value of the local pore thermal conductivity is then derived from the entire network and reported at each saturation level. It is important to note that the saturation of pores (and pore clusters) not belonging to the spanning cluster of the wetting phase (which connects the air and water reservoirs) is considered non-contributory to the thermal conduction. These isolated pores are surrounded by air-filled pores, effectively masking their heat conduction. For such pore unit cells, we assign the λ value of a dry pore unit cell.

To identify the continuous path of the wetting phase, including various isolated wetting phase clusters and the main spanning cluster, a search algorithm commonly used in computer vision and robotics is employed (Haralick &

TABLE 3 Best-matched pore network model (PNM) structural parameters.

Soil	n	c	μ	σ	R_{min} (μm)	R_{max} (μm)
F-75 Sand	0.727	0.165	4.45	2.696	14.701	112.798
12/20 Sand	2.565	0.986	6.946	1.127	0.059	227.31
River sand	0.015	0.116	5.505	2.696	13.929	112.798
SM1	2.022	0.405	3.771	1.57	5.985	154.668
SM2	0.919	0.039	3.648	1.005	4.352	275.071
SP	0.015	0.663	3.84	2.696	18.657	112.798
SP2	0.538	0.924	4.034	2.189	13.701	103.941
SP5	0.015	0.663	4.034	2.59	4.748	111.798

Shapiro, 1992; Sedgewick, 1998). The algorithm makes it possible to detect connected objects in an image.

Since the model calculates the local thermal conductivity of a soil unit cell embracing a pore, the term pore unit cell network model (PUCNM) is used hereafter to better convey the concept behind the calculations. To summarize, at first, saturations of different pores within the PNM are calculated, and then local λ values of the soil units are obtained based on the local saturations and upscaled by averaging through the network. The efficacy and appropriateness of the proposed approach for determining TCDC are assessed using various measures of performance as outlined in Table 2.

4 | RESULTS

The structural parameters of the best-matching PNMs for our eight soils are detailed in Table 3. Figure 4 shows the simulated SWRCs along with the experimental data. The optimized PNMs accurately replicated the SWRCs of the eight sandy soils, demonstrating the effectiveness of the selected structural parameters.

Figures 5 and 6 present the eight soils-simulated TCDCs as obtained with the pore unit cell network model (PUCNM) against those derived with the literature equations and experimental data. The figures show that the PUCNM estimates closely align with the experimental TCDC data, especially in the pendular regime. The other models within this regime deviate significantly from the experimental values, often underestimating them. The performance of the PUCNM is further contrasted in Figure 5a,b with the pore-scale model of Likos (2014b). The PUCNM approach provided much better TCDC estimates compared to the bundle of capillary tubes model used by Likos (2014b). In the capillary tube model, pores of the same size drain simultaneously at a specific matric suction, without considering the presence of both pore bodies and pore throats, thereby neglecting connectivity in the PNM. The PUCNM, on the other hand, incorporates both the pore body and pore throat elements and thus accounts for the connectivity between different pore unit cells. This allows for more precise estimates of local saturation and the thermal conductivity in especially the pendular moisture regime where λ has its lowest values (Figure 6). The PUCNM formulation, with its more comprehensive account of the natural soil geometrical and topological features, hence offers a more accurate representation than the simpler capillary tubes model.

To better understand the superior performance of the PUCNM pore-scale network model across all saturation regimes, especially in the pendular regime, an in-depth analysis of the wetting phase saturation evolution within the PNM was conducted. This included examining the local λ values of pores located within the spanning-wetting cluster of the samples (i.e., the continuous wetting phase cluster connecting the air and water reservoirs), and the ratio of the number of pores in the spanning-wetting phase cluster to the total number of pores (denoted as RPSC). These aspects are illustrated in Figure 7.

First and on top in Figure 7 are the simulated and experimental data of the TCDC of River sand, as well as the portions of all pores of the network that belong to the spanning-wetting cluster are depicted (denoted by RPSC). In the lower part of the figure, at each saturation, are two illustrations. One is the soil PNM at a certain soil saturation, with the corresponding local pore saturations presented in different colors. The second network shows the local λ values of pores in the spanning-wetting cluster and the extent of the spanning cluster in size. This illustration reveals a significant decrease in both the extent of the spanning-wetting phase cluster and the percentage of pores within this cluster at around 20% saturation, which marks the transition to the pendular regime, approximately corresponding to the residual water content in the classical SWRC models of Brooks and Corey (1964) and van Genuchten (1980). Consequently, the effective medium value of λ, calculated as the average of the local λ values in the PUCNM, is markedly reduced. Eventually, the continuous and spanning cluster of the wetting phase connecting the two reservoirs diminishes, causing the PUCNM-derived thermal conductivities to approach those of a dry soil.

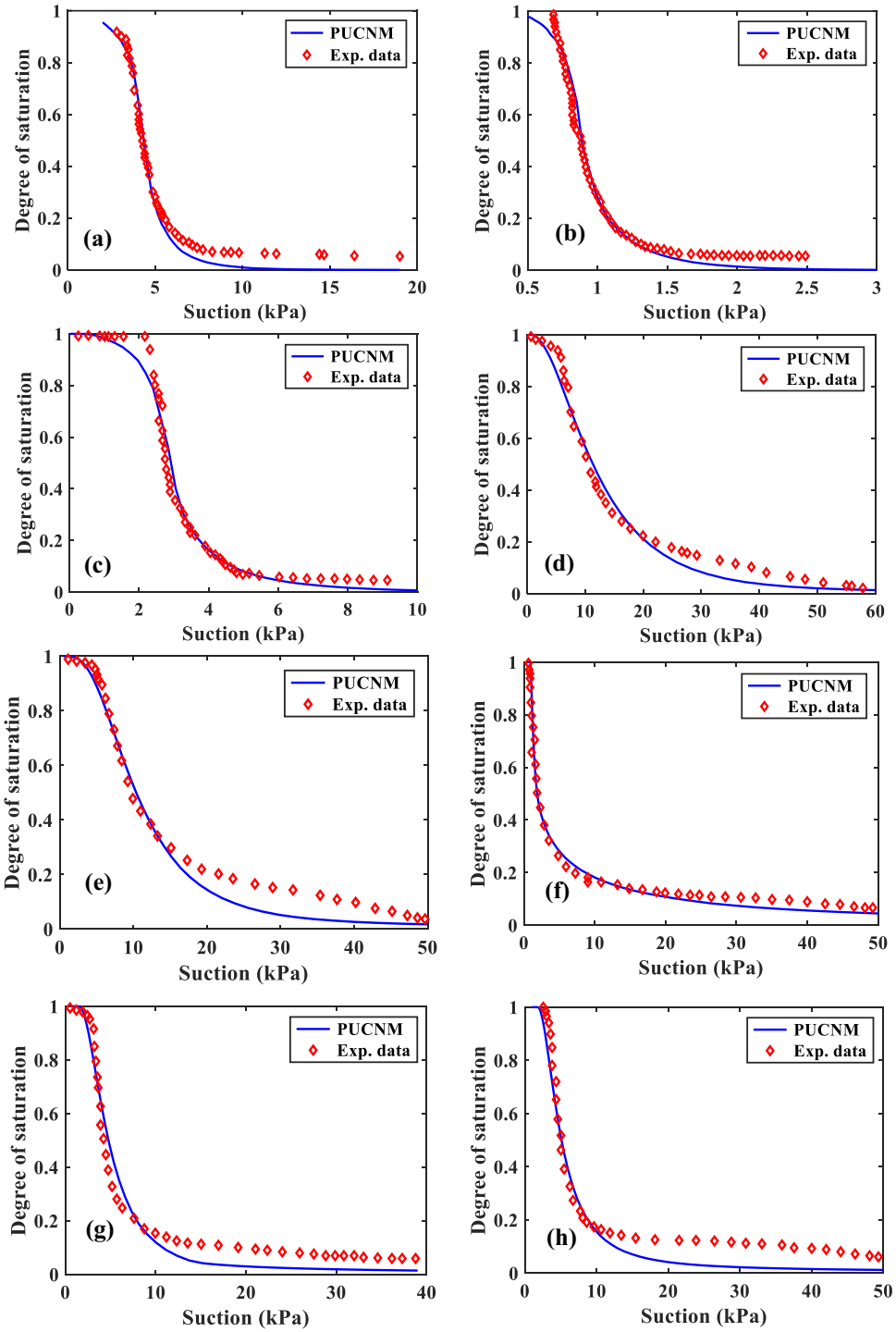

FIGURE 4 Pore unit cell network model (PUCNM) simulated and experimental data points of soil water retention curves (SWRCs) of various sandy soils: (a) F-75 sand, (b) 12/20 sand, (c) River sand, (d) SM1, (e) SM2, (f) SP, (g) SP2, and (h) SP5. PUCNM, pore unit cell network model.

Figure 8 presents, for the different approaches, the performance metrics in terms of the R^2, RMSE, and the MAPE. The analysis reveals that none of the models provided perfectly accurate TCDC estimates for all soils. The model by Hu et al. (2001) tended to overestimate experimental data, while the other models by Somerton et al. (1974), Johansen (1975), Côté and Konrad (2005), and Lu et al. (2007) generally underestimated the thermal conductivity. However, the PUCNM demonstrated a notable ability to capture the general trend of the TCDC experimental data across the different flow regimes, exhibiting the highest R^2 and lowest RMSE and MAPE values compared to the other approaches.

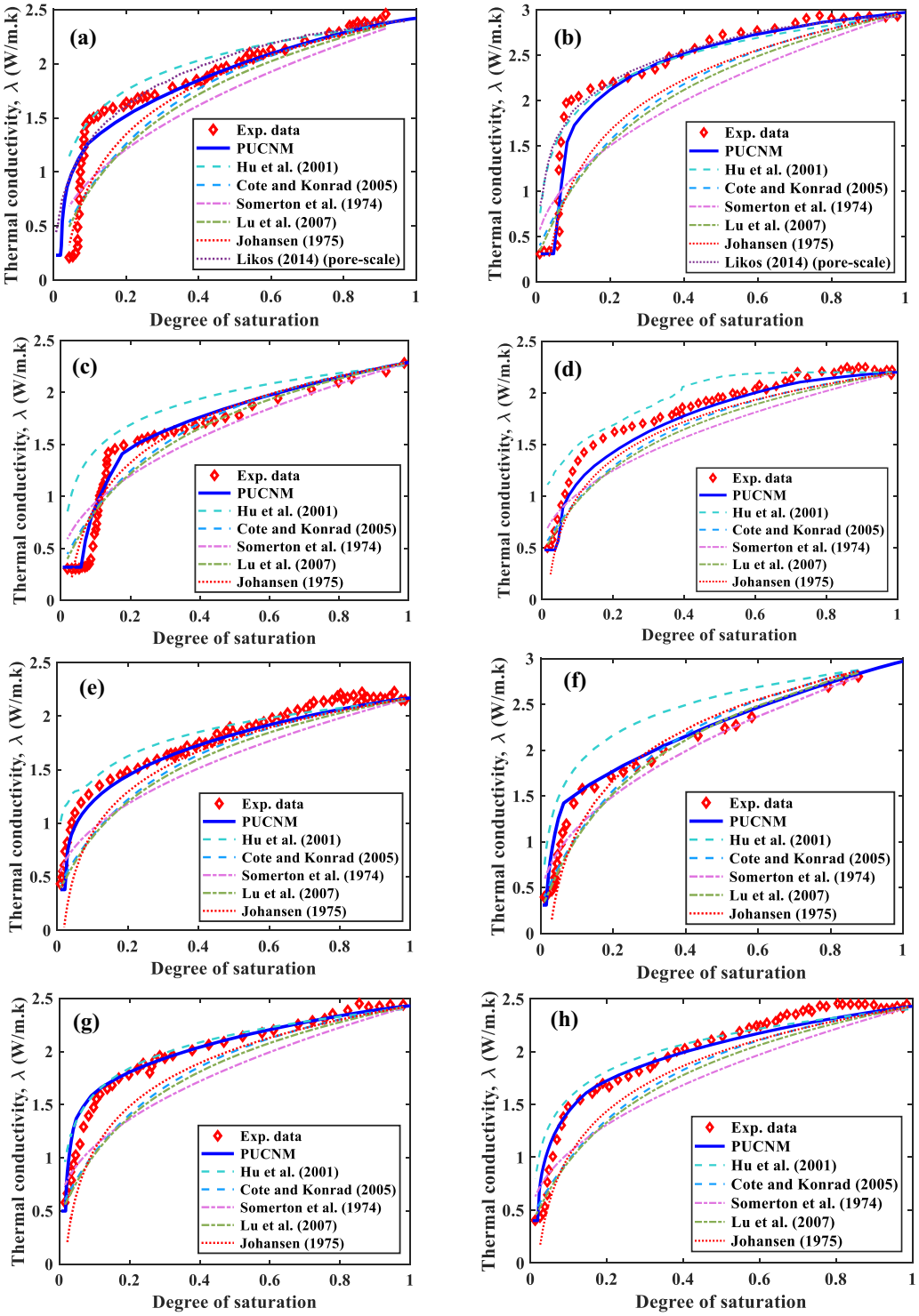

FIGURE 5 Calculated thermal conductivity drying curves (TCDCs) versus experimental data for soils (a) F-75 sand, (b) 12/20 sand, (c) River sand, (d) SM1, (e) SM2, (f) SP, (g) SP2, and (h) SP5 and comparisons with other models. PUCNM, pore unit cell network model. Likos (2014) stands for pore scale simulations of Likos (2014b).

5 | DISCUSSION OF THE RESULTS

Figure 7 illustrates that in coarse-grained soils, such as sandy soils, distinct regimes of the thermal conductivity varying with saturation are observable. The sharp decrease in the unsaturated thermal conductivity is notably marked by the transition from the funicular to the pendular regime. The PUCNM simulations show that the connected spanning cluster of the pore network begins to shrink at this transition. Specifically, the proportion of total pores in the network

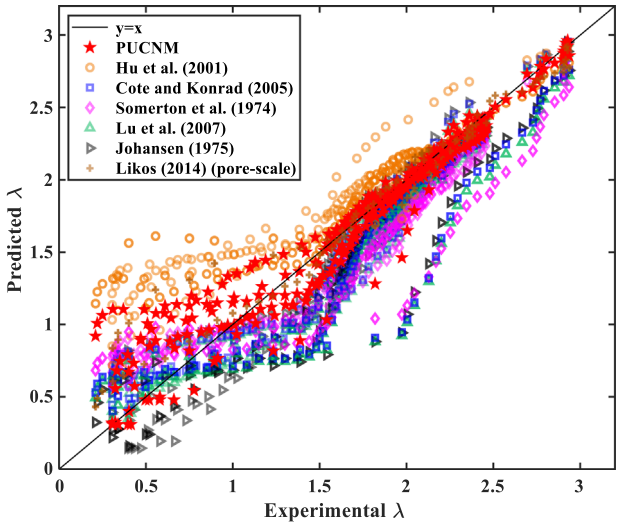

FIGURE 6 Predicted λ values of the thermal conductivity drying curves (TCDCs) versus experimental data for the eight sandy soils, estimations through other formulas and the pore-scale model of Likos (2014b).

that belong to this cluster, denoted by RPSC in Figure 7, starts to decrease. Once there is no connected wetting phase cluster, the thermal conductivity values remain unchanged. This direct correlation between heat flow and water flow is also evident in evaporation phenomena (Fu et al., 2024). Coussot (2000) utilized the concept of water connectivity loss in the pendular regime to define the second regime (often called the falling-rate regime) in evaporation curves. As air becomes trapped in the pores, water persists in the form of water bridges, causing the heat-conducting water pathways to narrow and eventually disconnect. Cho and Santamarina (2001) also identified the boundary between the pendular and funicular regimes as a critical point that defines different regimes for electrical conduction and chemical diffusion in unsaturated porous media.

In our study, we employed Equation (13) (determined from a quadratic parallel scheme as presented in Appendix A) to correlate the local saturation of pores with the thermal conductivity of a unit pore. The equation is somewhat similar to the function used by Côté and Konrad (2005). This raises the question what the outcome would be if the same function was applied to the global saturation of the network, instead of accounting for the local saturation of each pore and then upscaling. Figure 9 addresses this question by comparing PUCNM results with the predictions of Côté and Konrad (2005) for different values of the κ parameter in Equation (5), applied to the bulk network saturation. Results clearly show that the PUCNM calculations align more closely with the experimental data across all values of the κ parameter. This underscores the inability of traditional models to capture the critical role of the spanning cluster and its influence on the network thermal conductivity, thus highlighting the necessity of PNM. It also emphasizes the importance of considering the local saturation values of individual pores and their impact on a macroscopic parameter like the soil thermal conductivity.

In scenarios with varying grain size distributions, local pore saturations can differ significantly from the overall network saturation. Consequently, the average λ value derived from variable local saturations can substantially deviate from the thermal conductivity estimated directly from a single (bulk) network saturation value. Mathematically, for a nonlinear function f (e.g., for mapping saturation to λ), the expected value of the function for a set of input values (like saturation) does not equate to the function's value when applied to the average of the inputs, that tis, $E(f(s_i)) \neq f(E(s_i))$. This discrepancy highlights the critical role of pore-scale models in upscaling and accurately estimating macroscopic unsaturated properties such as the hydraulic and thermal conductivities.

Figure 10 explores the impact of the PNM structural parameters, notably the coordination number parameter (c) and the aspect ratio parameter (n), on thermal conductivity. Results suggest that a decreased threshold probability (indicating lower connectivity) leads to a higher saturation threshold for the onset of the decline in λ. In other words, less connected networks experience a reduction in the spanning cluster size at higher saturations. Similarly, increasing the aspect ratio to reflect smaller throat sizes implies a more gradual change in network saturation with suction until some high suction is reached. At this point, more extensive pore drainage occurs, causing the spanning cluster to retract and λ to decrease at higher saturations.

As can be seen, the aspect ratio parameter (n) significantly affects the unsaturated soil thermal conductivity. It should be noted that in the proposed approach, the aspect ratio parameter does not directly enter the calculations; instead, it affects the distribution of saturation within the soil PNM, thereby influencing the local thermal conductivities of soil pore unit cells and, ultimately, the bulk soil value of λ.

6 | MODEL LIMITATIONS, SCOPE OF APPLICATIONS, AND FUTURE OUTLOOK

The limitations of the proposed model, its cope of application, and potential for further developments can be discussed in light of different physical phenomena as well as soil characteristics, grouped into the following four items:

1. Temperature effects: The proposed model was formulated for the thermal conductivity of unsaturated sandy soils at ambient temperature. However, the thermal conductivity is known to vary with temperature (Campbell et al., 1994; de Vries, 1963; Hopmans & Dane, 1986a; Sepaskhah & Boersma, 1979; Xu et al., 2019). Particularly, in

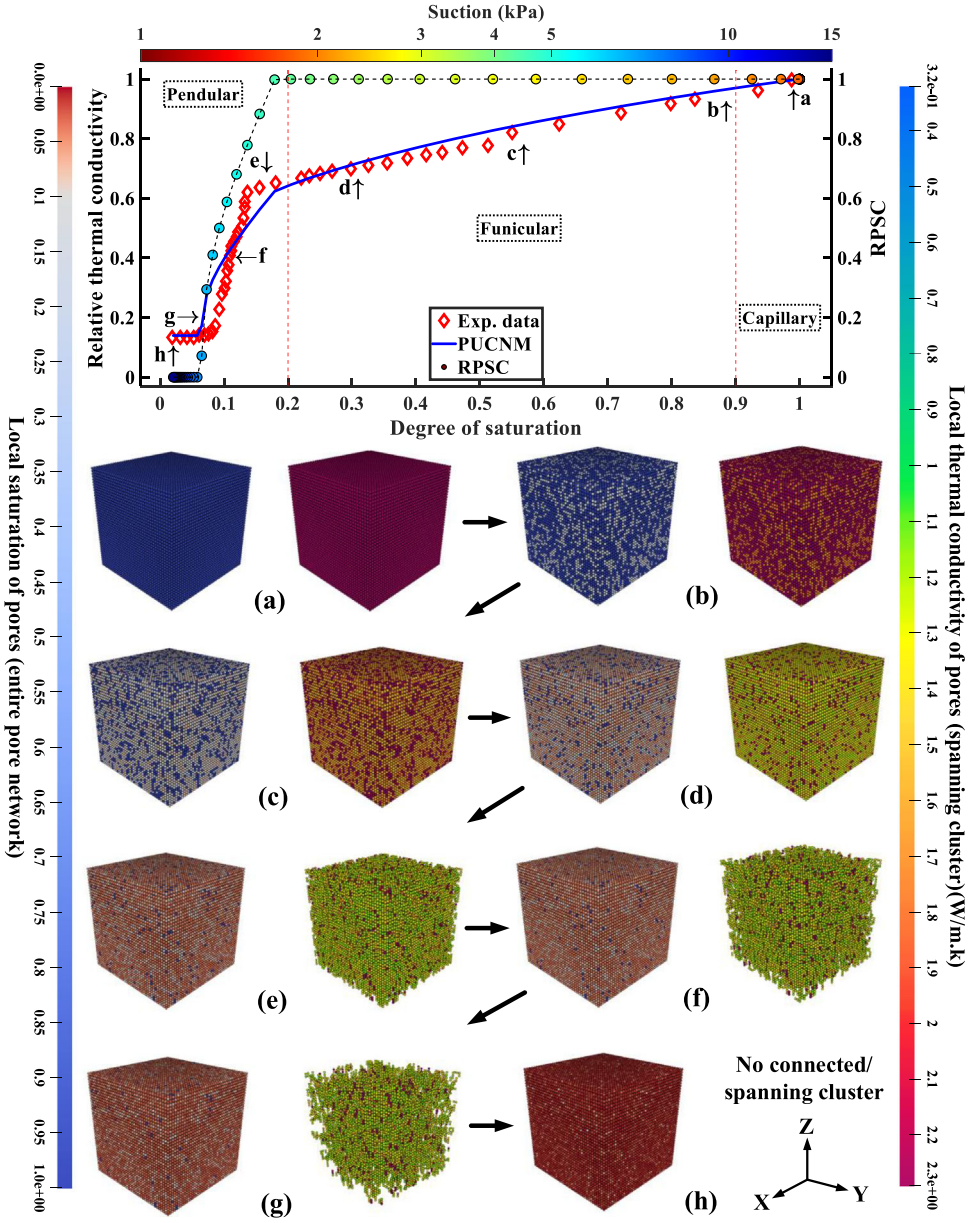

FIGURE 7 Evolution of local saturation (refer to the PNMs illustrated in the first and third columns) and spanning-wetting phase cluster local thermal conductivities in the PUCNM (see the networks presented in the second and fourth columns) during drying of River sand at different saturations: (a) $S = 1.0$, (b) $S = 0.88$, (c) $S = 0.54$, (d) $S = 0.28$, (e) $S = 0.14$, (f) $S = 0.1$, (g) $S = 0.08$, and (h) $S = 0.03$. RPSC gives the ratio of the number of pores in the spanning-wetting phase cluster to the total number of pores. PUCNM, pore unit cell network model.

medium- to fine-textured soils, vapor transfer has been reported to occur at high temperatures (Sepaskhah & Boersma, 1979), while latent heat transfer may become a significant portion of total heat transfer at relatively low water contents and high temperatures (Tarnawski & Leong, 2000). To more precisely estimate the thermal conductivity at higher temperatures, these phenomena must be accounted for (i.e., at high temperatures, the vapor conductivity should be substituted for air conductivity when determining the unit cell thermal conductivity in the PUCNM). Therefore, the development of the model for predicting the unsaturated thermal conductivity at higher temperatures, especially for fine-grained soils, requires careful incorporation of relevant physics (such as vapor transfer and temperature-dependent changes in soil structure, such as the double layer thickness, which indirectly affects the SWRC parameters as discussed by Nimmo and Miller (1986), Hopmans and Dane (1986b), Grant and Salehzadeh (1996), François and Ettahiri (2012), and Khaksar et al. (2015), among others).

2. Hysteresis effects: The PUCNM technique was evaluated for determining the unsaturated thermal conductivity

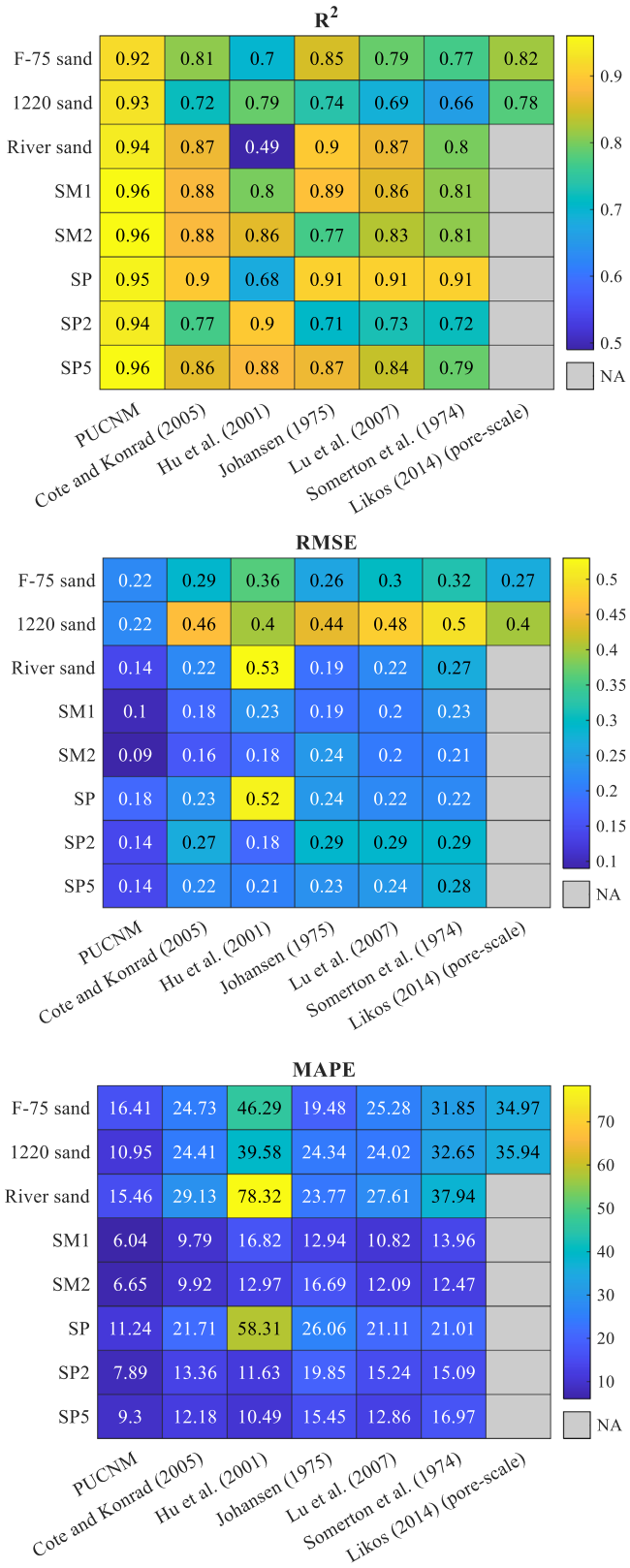

FIGURE 8 Comparison of the R^2, root mean squared error (RMSE), and mean absolute percentage error (MAPE) performance measures of the various models in describing the thermal conductivity drying curves (TCDCs) of eight sandy soils. NA, not available. Likos (2014) stands for pore scale simulations of Likos (2014b).

during drying. The model effectively revealed how wetting phase connectivity and the extent of the connected wetting phase cluster influence thermal conductivity changes across different capillary regimes, especially during the transition from a funicular to a pendular regime. We found that the formation of entrapped air and a reduction in network connectivity lead to a decrease in unsaturated thermal conductivity. However, the amount of entrapped air varies from a soil undergoing drying to the same soil at the same saturation reached through wetting or scanning processes. This variation results in different air and water saturations across the soil pore network, a key aspect of the hysteresis phenomenon (Chen et al., 2015; Kaluarachchi & Parker, 1987; Lenhard & Parker, 1987; Poulovassilis, 1970; Stonestrom & Rubin, 1989). Sharma and Mohamed (2003) noted that the amount of entrapped air is determined by the reversal degree of saturation during a drying-wetting cycle, which specifies the saturation level at the cycle's turning point. Variations in air entrapment significantly impact water flow (Fayer & Hillel, 1986a, 1986b; Stauffer & Dracos, 1984) and, due to a strong correlation with air-filled porosity, also affect the unsaturated thermal conductivity (Ochsner et al., 2001). Experimental studies have shown that the degree of hysteresis in unsaturated thermal conductivity curves heavily depends on soil structure and soil type (Ali et al., 2014; Cardoso et al., 2018; Farouki, 1981; Nguyen et al., 2017, 2018; Smits et al., 2010; Tang et al., 2008; Vu et al., 2023; Xu et al., 2020; Zhou et al., 2019). Soils with different grain size distributions and types, including those prepared in undisturbed or compacted states, exhibit varying pore structures, leading to different levels of air entrapment during drying-wetting cycles and, consequently, varying degrees of hysteresis in the unsaturated thermal conductivity (λ). Given that PUCNM incorporates elements of pore bodies and pore throats, which govern the processes of drying and wetting, this model appears to be a promising tool for investigating unsaturated thermal conductivity in future studies on hysteresis effects. However, the model must incorporate fluid phase displacement mechanisms that govern wetting and scanning processes, such as cooperative pore filling and snap-off during imbibition (Mirghafari et al., 2024; Rostami et al., 2015).

3. The role of soil structure, connectivity and tortuosity: We validated the proposed model using data from coarse-grained soils, specifically sandy soils. Fine-grained soils, especially those that are structured and aggregated, generally possess a more complex soil pore network comprising two distinct pore categories: intra- and inter-aggregate pores. Studies have demonstrated that heat transfer decreases as aggregate size increases (Usowicz et al., 2013; Zhou et al., 2019). Consequently, the path

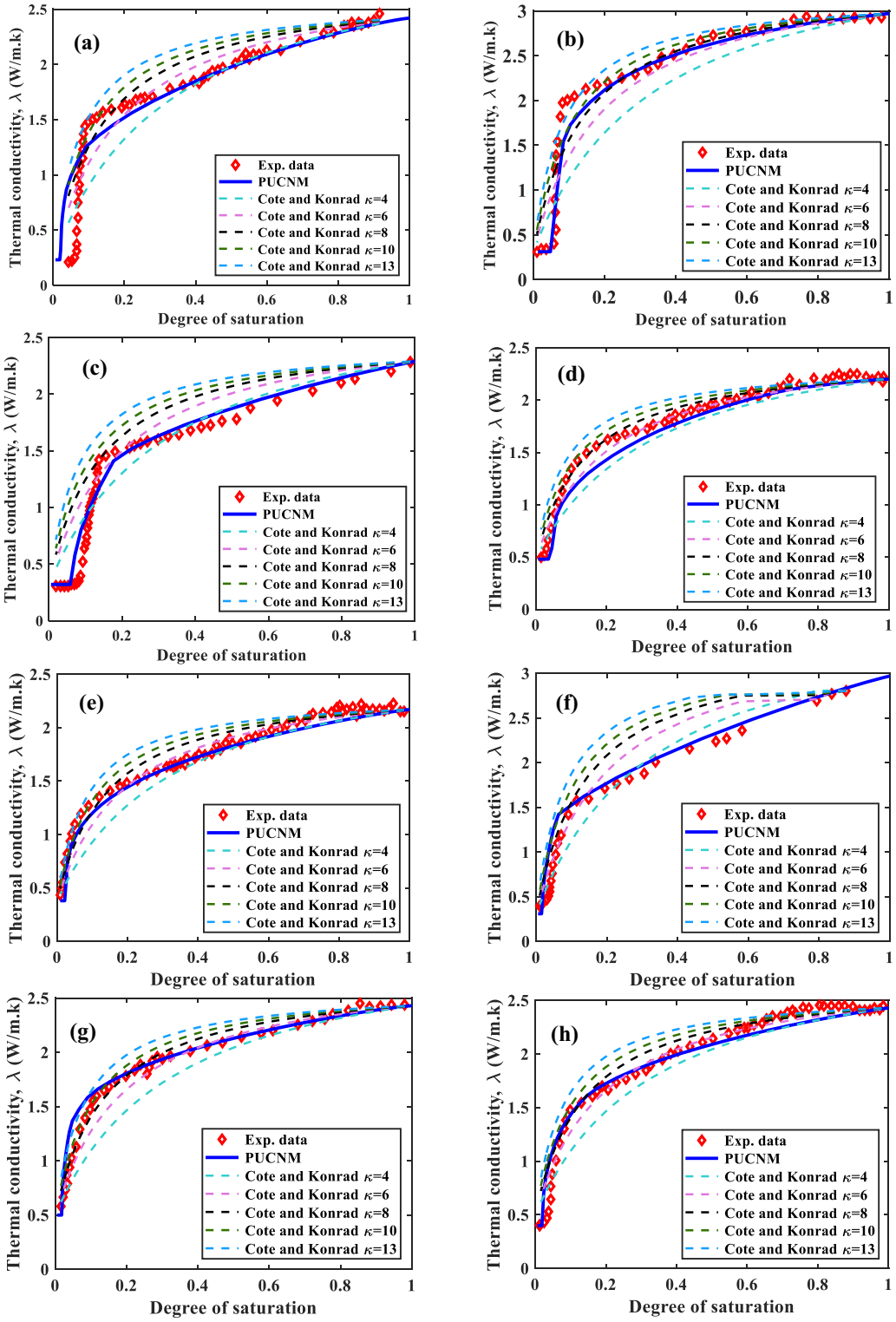

FIGURE 9 Performance of pore unit cell network model (PUCNM) compared to direct estimation of the thermal conductivity using the Côté and Konrad (2005) model with different κ values for soils (a) F-75 sand, (b) 12/20 sand, (c) River sand, (d) SM1, (e) SM2, (f) SP, (g) SP2, and (h) SP5.

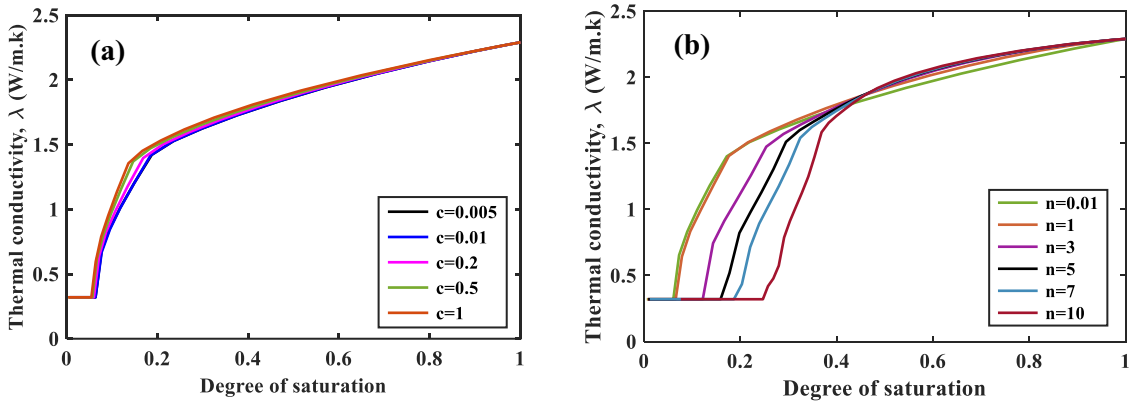

FIGURE 10 Sensitivity analysis of simulated thermal conductivity drying curves (TCDCs) for different values of pore unit cell network model (PUCNM) structural parameters (a) the coordination number parameter (c) and (b) the aspect ratio parameter (n).

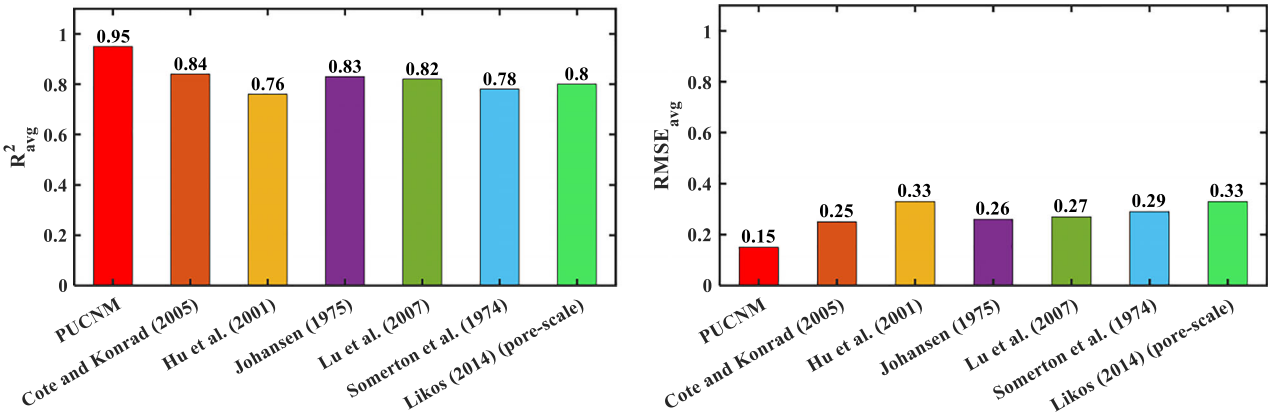

FIGURE 11 Comparison of the average of R^2 and root mean squared error (RMSE) of all equations and the pore unit cell network model (PUCNM) model used in this study.

of heat transfer and its tortuosity are influenced by the size of aggregates, or more precisely, by the distribution of intra- and interaggregate pore sizes. To extend the proposed PUCNM technique to other soil types, it is essential to account for variations in soil pore structure and to consider a wider range of pore sizes, extending down to nanometer-scale pores. The development of multiscale pore-scale models, a practice already underway in fields such as petroleum engineering for studying two-phase flow in shales (Alafnan & Yucel Akkutlu, 2020; Cui et al., 2019), offers valuable insights for investigating the physical properties of fine-grained structured soils.

4. Surface water adsorption: To adapt the PUCNM for fine-grained soils, it is crucial to account for the presence of adsorbed water. The current model, designed primarily for sandy soils, considers only mobile and capillary water within a single pore class. In fine-grained soils, distinguishing between adsorbed (including hydration water) and capillary (mobile) water is essential (Dong et al., 2015; Lu, 2016). Hydration water does not enhance connectivity among grains, which explains the pronounced stasis behavior or the extended tail in the unsaturated thermal conductivity profiles of fine-grained soils. As the fine-grained soil content, especially clay, increases, so does the length of this tail and the corresponding threshold water content. Exceeding this threshold leads to an increase in the mobile water content, thereby establishing connectivity between grains and significantly enhancing the overall soil thermal conductivity. The soil's plasticity, the tendency of minerals to adsorb water, and the specific surface area of fine soil particles govern this behavior. Recent advancements in nuclear magnetic resonance (NMR) have enabled the quantification of adsorbed water in unsaturated porous media such as wood and soil (Cocusse et al., 2022; Eizaguirre et al., 2024). These advancements in dynamic NMR relaxometry, combined with dynamic X-ray (or neutron) tomography together with thermal imaging, provide insights into the local heat paths and their development within the soil porous medium. Until these advanced experimental techniques become more accessible, advancements in pore-scale models such as PUCNM

are vital for understanding the dynamics of the thermal conductivity in unsaturated porous media.

7 | CONCLUSIONS

In this study, we utilized a PUCNM to estimate the TCDC of coarse-textured soils. The model demonstrated promising accuracy in estimating the unsaturated TCDC of sands as indicated by the average R^2 and RMSE values across all studied soils (Figure 11). The PUCNM results showed an impressive R^2 of 95%, indicating highly accurate TCDC estimations across the full range of saturation. The model excelled especially in the pendular regime (saturations below 20%), where other models failed to accurately describe the experimental data. The enhanced performance of the proposed model is due to its ability to differentiate between disconnected wetting clusters and pores situated on the spanning (continuous) water cluster within the soil PNM. Since the thermal conductivity (λ) of isolated and disconnected wetting clusters is obscured by surrounding air-filled pores, the extent of the spanning cluster and the percentage of pores belonging to this cluster significantly control the overall unsaturated soil λ value. A marked shrinkage of the spanning cluster in the pendular regime leads here then to a substantial decrease in the unsaturated λ.

The PUCNM results also underscored the importance of pore-level saturation and the resulting local λ. The model leads to more accurate global λ estimates compared to models using bulk network saturation. The relevance of pore-scale modeling, as demonstrated by PUCNM, in upscaling macroscopic characteristics such as the TCDC is evident from our findings.

Future research should focus on incorporating various pore-scale displacement processes to more accurately capture fluid saturation and thermal conductivity changes throughout the entire hydraulic cycle (i.e., to enable simulating unsaturated thermal properties in not only drying but also in wetting curves). Using advanced imaging techniques, such as thermal imaging combined with neutron tomography and X-ray computed tomography, together with dynamic NMR relaxometry, will provide more insights into heat conduction processes in the unsaturated zone across different saturation regimes. With the advent of 4D tomography and thermal imaging, unique opportunities arise for observing these processes in real time. Until such advancements are widespread, the insights gained from PNM can greatly enhance our understanding of unsaturated soil pore-scale characteristics and their impact on macroscopic properties. The PUCNM approach in this study was applied to very coarse-textured (sandy) soils. Its broader applicability, such as to fine-grained soils, requires the incorporation of corner and film flow in the pore throats and the use of multi-structural soil PNMs that consider a broader range of pore sizes (e.g., inter- and intra-aggregate pores typical of aggregated or structured media).

AUTHOR CONTRIBUTIONS

Rasoul Mirghafari: Investigation; methodology; software; validation; visualization; writing—original draft; writing—review and editing. **Amir Hossein Helforoosh**: Investigation; software; validation. **Ehsan Nikooee**: Conceptualization; methodology; software; supervision; writing—original draft; writing—review and editing. **Ghassem Habibagahi**: Supervision; writing—review and editing. **Amir Raoof**: Methodology; writing—review and editing. **Martinus Theodorus van Genuchten**: Writing—review and editing.

CONFLICT OF INTEREST STATEMENT

The authors declare no conflicts of interest.

ORCID

Ehsan Nikooee https://orcid.org/0000-0003-2365-1132
Martinus Theodorus van Genuchten https://orcid.org/0000-0003-1654-8858

REFERENCES

Abu-Hamdeh, N. H. (2000). Effect of tillage treatments on soil thermal conductivity for some Jordanian clay loam and loam soils. *Soil and Tillage Research*, *56*(3–4), 145–151. https://doi.org/10.1016/S0167-1987(00)00129-X

Abu-Hamdeh, N. H., & Reeder, R. C. (2000). Soil thermal conductivity effects of density, moisture, salt concentration, and organic matter. *Soil Science Society of America Journal*, *64*(4), 1285–1290. https://doi.org/10.2136/sssaj2000.6441285x

Acharya, R. C., van der Zee, S. E. A. T. M., & Leijnse, A. (2004). Porosity–permeability properties generated with a new 2-parameter 3D hydraulic pore-network model for consolidated and unconsolidated porous media. *Advances in Water Resources*, *27*, 707–723. https://doi.org/10.1016/j.advwatres.2004.05.002

Akrouch, G. A., Sánchez, M., & Briaud, J. L. (2016). An experimental, analytical and numerical study on the thermal efficiency of energy piles in unsaturated soils. *Computers and Geotechnics*, *71*, 207–220. https://doi.org/10.1016/j.compgeo.2015.08.009

Alafnan, S., & Yucel Akkutlu, I. (2020). The transport mechanisms and dynamics of shale via multiscale multiphysics pore network modeling. *Journal of Energy Resources Technology*, *142*(9), 093003. https://doi.org/10.1115/1.4046522

Ali, A., Mohamed, M., Aal, M. A., Schellart, A., & Tait, S. (2014). Thermal and hydraulic properties of sandy soils during drying and wetting cycles. *New frontiers in geotechnical engineering* (pp. 129–138). ASCE.

ASTM. (1985). *Classification of soils for engineering purposes: Annual book of ASTM standards* (D 2487-83, Vol. 04). American Society for Testing and Materials.

Bayat, H., Ebrahimzadeh, G., & Mohanty, B. P. (2021). Investigating the capability of estimating soil thermal conductivity using topographical attributes for the Southern Great Plains, USA. *Soil and Tillage Research*, *206*, 104811. https://doi.org/10.1016/j.still.2020.104811

Brooks, R., & Corey, T. (1964). *Hydraulic properties of porous media* (Hydrology Papers No. 3). Colorado State University Fort Collins Colorado.

Campbell, G. S., Jungbauer, J. D., Jr, Bidlake, W. R., & Hungerford, R. D. (1994). Predicting the effect of temperature on soil thermal conductivity. *Soil Science*, *158*(5), 307–313. https://doi.org/10.1097/00010694-199411000-00001

Caon, L., Vallejo, V. R., Ritsema, C. J., & Geissen, V. (2014). Effects of wildfire on soil nutrients in Mediterranean ecosystems. *Earth-Science Reviews*, *139*, 47–58. https://doi.org/10.1016/j.earscirev.2014.09.001

Cardoso, R., Sousa, M., & Vieira, A. (2018). Suction effect on the thermal properties of compacted kaolin. In *7th International conference on unsaturated soils*. International Society for Soil Mechanics and Geotechnical Engineering. https://www.issmge.org/publications/publication/suction-effect-on-the-thermal-properties-of-compacted-kaolin

Chen, P., Wei, C., & Ma, T. (2015). Analytical model of soil-water characteristics considering the effect of air entrapment. *International Journal of Geomechanics*, *15*(6), 04014102. https://doi.org/10.1061/(ASCE)GM.1943-5622.0000462

Cho, G. C., & Santamarina, J. C. (2001). Unsaturated particulate materials—Particle-level studies. *Journal of Geotechnical and Geoenvironmental Engineering*, *127*(1), 84–96. https://doi.org/10.1061/(asce)1090-0241(2001)127:1(84)

Cocusse, M., Rosales, M., Maillet, B., Sidi-Boulenouar, R., Julien, E., Caré, S., & Coussot, P. (2022). Two-step diffusion in cellular hygroscopic (vascular plant-like) materials. *Science Advances*, *8*(19), eabm7830. https://doi.org/10.1126/sciadv.abm7830

Conant, R. T., Ryan, M. G., Ågren, G. I., Birge, H. E., Davidson, E. A., Eliasson, P. E., Evans, S. E., Frey, S. D., Giardina, C. P., Hopkins, F. M., Hyvönen, R., Kirschbaum, M. U. F., Lavallee, J. M., Leifeld, J., Parton, W. J., Megan Steinweg, J., Wallenstein, M. D., Martin Wetterstedt, J. Å., & Bradford, M. A. (2011). Temperature and soil organic matter decomposition rates–synthesis of current knowledge and a way forward. *Global Change Biology*, *17*(11), 3392–3404. https://doi.org/10.1111/j.1365-2486.2011.02496.x

Cosenza, P., Guérin, R., & Tabbagh, A. (2003). Relationship between thermal conductivity and water content of soils using numerical modelling. *European Journal of Soil Science*, *54*(3), 581–588. https://doi.org/10.1046/j.1365-2389.2003.00539.x

Côté, J., & Konrad, J. M. (2005). A generalized thermal conductivity model for soils and construction materials. *Canadian Geotechnical Journal*, *42*(2), 443–458. https://doi.org/10.1139/t04-106

Coussot, P. (2000). Scaling approach of the convective drying of a porous medium. *The European Physical Journal B—Condensed Matter and Complex Systems*, *15*(3), 557–566. https://doi.org/10.1007/s100510051160

Cui, R., Feng, Q., Chen, H., Zhang, W., & Wang, S. (2019). Multiscale random pore network modeling of oil-water two-phase slip flow in shale matrix. *Journal of Petroleum Science and Engineering*, *175*, 46–59. https://doi.org/10.1016/j.petrol.2018.12.026

Daneshian, B., Habibagahi, G., & Nikooee, E. (2021). Determination of unsaturated hydraulic conductivity of sandy soils: A new pore network approach. *Acta Geotechnica*, *16*, 449–466. https://doi.org/10.1007/s11440-020-01088-3

de Vries, D. A. (1963). Thermal properties of soils. In W. R. Van Wijk (Ed.), *Physics of plant environment* (pp. 210–235). North-Holland.

Dong, Y., McCartney, J. S., & Lu, N. (2015). Critical review of thermal conductivity models for unsaturated soils. *Geotechnical and Geological Engineering*, *33*, 207–221. https://doi.org/10.1007/s10706-015-9843-2

Eizaguirre, P., Tang, A. M., Maillet, B., Sidi-Boulenouar, R., Talandier, J., Pereira, J.-M., Vu, M. N., Chabot, B., Dangla, P., Bornert, M., & Aimedieu, P. (2024). Exploring two regimes of water mobility in unsaturated expansive clay using NMR relaxometry. *Applied Clay Science*, *251*, 107324. https://doi.org/10.1016/j.clay.2024.107324

Farouki, O. (1981). *Thermal properties of soils*. US Army Corps of Engineers, Cold Regions Research and Engineering Laboratory.

Fayer, M. J., & Hillel, D. (1986a). Air encapsulation: I. Measurement in a field soil. *Soil Science Society of America Journal*, *50*(3), 568–572. https://doi.org/10.2136/sssaj1986.03615995005000030005x

Fayer, M. J., & Hillel, D. (1986b). Air encapsulation: II. Profile water storage and shallow water table fluctuations. *Soil Science Society of America Journal*, *50*(3), 572–577. https://doi.org/10.2136/sssaj1986.03615995005000030006x

Fedaoui, K., Madani, S., & KANIT, T. (2016). Prediction of effective thermal conductivity of heterogeneous random multi-phase composites. *UPB Scientific Bulletin Series D: Mechanical Engineering*, *78*(3), 91–100.

Flannigan, M. D., Stocks, B. J., & Wotton, B. M. (2000). Climate change and forest fires. *Science of the Total Environment*, *262*(3), 221–229. https://doi.org/10.1016/S0048-9697(00)00524-6

François, B., & Ettahiri, S. (2012). Role of the soil mineralogy on the temperature dependence of the water retention curve. *Unsaturated soils: Research and applications* (Vol. 1, pp. 173–178). Springer.

Fu, Y., Ghanbarian, B., Horton, R., & Heitman, J. (2024). New insights into the correlation between soil thermal conductivity and water retention in unsaturated soils. *Vadose Zone Journal*, *23*(1), e20297. https://doi.org/10.1002/vzj2.20297

Gamage, D. N. V., Biswas, A., & Strachan, I. B. (2019). Spatial variability of soil thermal properties and their relationships with physical properties at field scale. *Soil and Tillage Research*, *193*, 50–58. https://doi.org/10.1016/j.still.2019.05.012

Ghanbarian, B., & Daigle, H. (2016). Thermal conductivity in porous media: Percolation-based effective-medium approximation. *Water Resources Research*, *52*, 295–314. https://doi.org/10.1002/2015WR017236

Grant, S. A., & Salehzadeh, A. (1996). Calculation of temperature effects on wetting coefficients of porous solids and their capillary pressure functions. *Water Resources Research*, *32*(2), 261–270. https://doi.org/10.1029/95WR02915

Haralick, R. M., & Shapiro, L. G. (1992). *Computer and robot vision*. Addison-Wesley.

Hayashi, M., Goeller, N., Quinton, W. L., & Wright, N. (2007). A simple heat-conduction method for simulating the frost-table depth in hydrological models. *Hydrological Processes: An International Journal*, *21*(19), 2610–2622. https://doi.org/10.1002/hyp.6792

He, H., Liu, L., Dyck, M., Si, B., & Lv, J. (2021). Modelling dry soil thermal conductivity. *Soil and Tillage Research*, *213*, 105093. https://doi.org/10.1016/j.still.2021.105093

Heinze, J., Gensch, S., Weber, E., & Joshi, J. (2017). Soil temperature modifies effects of soil biota on plant growth. *Journal of Plant Ecology*, *10*(5), 808–821.

Hirabayashi, Y., Kanae, S., Emori, S., Oki, T., & Kimoto, M. (2008). Global projections of changing risks of floods and droughts in a changing climate. *Hydrological Sciences Journal*, *53*(4), 754–772. https://doi.org/10.1623/hysj.53.4.754

Hopmans, J. W., & Dane, J. H. (1986a). Thermal conductivity of two porous media as a function of water content, temperature, and density. *Soil Science*, *142*(4), 187–195. https://doi.org/10.1097/00010694-198610000-00001

Hopmans, J. W., & Dane, J. H. (1986b). Temperature dependence of soil water retention curves. *Soil Science Society of America Journal*, *50*(3), 562–567. https://doi.org/10.2136/sssaj1986.03615995005000030004x

Hu, X. J., Du, J. H., Lei, S. Y., & Wang, B. X. (2001). A model for the thermal conductivity of unconsolidated porous media based on capillary pressure-saturation relation. *International Journal of Heat and Mass Transfer*, *44*(1), 247–251. https://doi.org/10.1016/S0017-9310(00)00079-X

Jia, G. S., Tao, Z. Y., Meng, X. Z., Ma, C. F., Chai, J. C., & Jin, L. W. (2019). Review of effective thermal conductivity models of rock-soil for geothermal energy applications. *Geothermics*, *77*, 1–11. https://doi.org/10.1016/j.geothermics.2018.08.001

Joekar-Niasar, V., Hassanizadeh, S. M., & Dahle, H. K. (2010). Non-equilibrium effects in capillarity and interfacial area in two-phase flow: Dynamic pore-network modelling. *Journal of Fluid Mechanics*, *655*, 38–71. https://doi.org/10.1017/S0022112010000704

Johansen, O. (1975). *Varmeledningsevne av jordarter* [Doctoral dissertation, Norwegian Institute of Technology].

Johansen, O. (1977). *Thermal conductivity of soils*. Cold Regions Research and Engineering Laboratory.

Kaluarachchi, J. J., & Parker, J. C. (1987). Effects of hysteresis with air entrapment on water flow in the unsaturated zone. *Water Resources Research*, *23*(10), 1967–1976. https://doi.org/10.1029/WR023i010p01967

Kersten, M. S. (1949). *Thermal properties of soils* (Bulletin No. 28). Engineering Experiment Station, Institute of Technology, University of Minnesota.

Khaksar, H., Habibagahi, G., & Nikooee, E. (2013). SWRC modeling in unsaturated soils: A pore network approach. In *Poromechanics V: Proceedings of the Fifth Biot Conference on Poromechanics* (pp. 1570–1579). ASCE. https://ascelibrary.org/doi/10.1061/9780784412992.186

Khaksar, H., Nikooee, E., Habibagahi, G., & Hassanizadeh, S. M. (2015). Modeling temperature effects on soil water retention curve: A pore network approach. *Geotechnical engineering for infrastructure and development* (pp. 3267–3272). ICE. https://www.icevirtuallibrary.com/doi/abs/10.1680/ecsmge.60678.vol6.511

Khaledi, S., Delbari, M., Galavi, H., Bagheri, H., & Chari, M. M. (2023). Effects of biochar particle size, biochar application rate, and moisture content on thermal properties of an unsaturated sandy loam soil. *Soil and Tillage Research*, *226*, 105579. https://doi.org/10.1016/j.still.2022.105579

Lehmann, P., Stahli, M., Papritz, A., Gygi, A., & Fluhler, H. (2003). A fractal approach to model soil structure and to calculate thermal conductivity of soils. *Transport in Porous Media*, *52*, 313–332. https://doi.org/10.1023/A:1023595527999

Lei, G., Yu, X., Li, T., Habibzadeh-Bigdarvish, O., Wang, X., Mrinal, M., & Luo, C. (2020). Feasibility study of a new attached multi-loop CO_2 heat pipe for bridge deck de-icing using geothermal energy. *Journal of Cleaner Production*, *275*, 123160. https://doi.org/10.1016/j.jclepro.2020.123160

Lenhard, R. J., & Parker, J. C. (1987). A model for hysteretic constitutive relations governing multiphase flow: 2. Permeability-saturation relations. *Water Resources Research*, *23*(12), 2197–2206. https://doi.org/10.1029/WR023i012p02197

Likos, W. J. (2014a). Modeling thermal conductivity dryout curves from soil-water characteristic curves. *Journal of Geotechnical and Geoenvironmental Engineering*, *140*(5), 04013056. https://doi.org/10.1061/(ASCE)GT.1943-5606.0001078

Likos, W. J. (2014b). Pore-scale model for thermal conductivity of unsaturated sand. *Geotechnical and Geological Engineering*, *33*(2), 179–192. https://doi.org/10.1007/s10706-014-9744-9

Lu, N. (2016). Generalized soil water retention equation for adsorption and capillarity. *Journal of Geotechnical and Geoenvironmental Engineering*, *142*(10), 04016051. https://doi.org/10.1061/(ASCE)GT.1943-5606.0001524

Lu, S., Ren, T., Gong, Y., & Horton, R. (2007). An improved model for predicting soil thermal conductivity from water content at room temperature. *Soil Science Society of America Journal*, *71*(1), 8–14. https://doi.org/10.2136/sssaj2006.0041

McKersie, B. (2015). Planning for food security in a changing climate. *Journal of Experimental Botany*, *66*(12), 3435–3450. https://doi.org/10.1093/jxb/eru547

Mirghafari, R., Nikooee, E., Raoof, A., & Habibagahi, G. (2024). Determination of a pedotransfer function for specific air water interfacial area in sandy soils: A pore network-informed multigene genetic programming approach. *Vadose Zone Journal*, e20352. https://doi.org/10.1002/vzj2.20352

Moradshahi, A., Faizal, M., Bouazza, A., & McCartney, J. S. (2021). Effect of nearby piles and soil properties on thermal behaviour of a field-scale energy pile. *Canadian Geotechnical Journal*, *58*(9), 1351–1364. https://doi.org/10.1139/cgj-2020-0353

Mustamo, P., Ronkanen, A. K., Berglund, Ö., Berglund, K., & Kløve, B. (2019). Thermal conductivity of unfrozen and partially frozen managed peat soils. *Soil and Tillage Research*, *191*, 245–255. https://doi.org/10.1016/j.still.2019.02.017

Newson, T. A., & Brunning, P. (2004). Thermal conductivity of deepwater offshore sediments. *International Journal of Offshore and Polar Engineering*, *14*(4), 310–314.

Nguyen, V. T., Heindl, H., Frost, J. D., Pereira, J. M., & Tang, A. M. (2018). *Suction and thermal conductivity of unsaturated loess from Northern France*. UNSAT. https://www.issmge.org/uploads/publications/62/63/4-17.UNSAT2018_085.pdf

Nguyen, V. T., Heindl, H., Pereira, J. M., Tang, A. M., & Frost, J. D. (2017). Water retention and thermal conductivity of a natural unsaturated loess. *Géotechnique Letters*, *7*(4), 286–291. https://doi.org/10.1680/jgele.17.00037

Nikooee, E., Habibagahi, G., Khaksar, H., Hassanizadeh, S., & Raoof, A. (2014). Pore network modeling of unsaturated soils: Fundamentals, recent advancements and future perspectives. *Numerical Methods in Geotechnical Engineering-NUMGE*, *2014*, 1007–1012. https://doi.org/10.1201/b17017-179

Nimmo, J. R., & Miller, E. E. (1986). The temperature dependence of isothermal moisture vs. potential characteristics of soils. *Soil Science Society of America Journal*, *50*(5), 1105–1113. https://doi.org/10.2136/sssaj1986.03615995005000050004x

Ochsner, T. E., Horton, R., & Ren, T. (2001). A new perspective on soil thermal properties. *Soil Science Society of America Journal*, *65*(6), 1641–1647. https://doi.org/10.2136/sssaj2001.1641

Ocłoń, P. (2021). The effect of soil thermal conductivity and cable ampacity on the thermal performance and material costs of under-

ground transmission line. *Energy*, *231*, 120803. https://doi.org/10.1016/j.energy.2021.120803

Oh, H. (2014). *Thermal resistivity dry-out curves for thirteen sandy soils* [Master's thesis, University of Wisconsin-Madison].

Patwa, D., Bordoloi, U., Dubey, A. A., Ravi, K., Sekharan, S., & Kalita, P. (2022). Energy-efficient biochar production for thermal backfill applications. *Science of the Total Environment*, *833*, 155253. https://doi.org/10.1016/j.scitotenv.2022.155253

Population. United Nations. (2023). https://www.un.org/en/global-issues/population

Poulovassilis, A. (1970). The effect of the entrapped air on the hysteresis curves of a porous body and on its hydraulic conductivity. *Soil Science*, *109*(3), 154–162. https://doi.org/10.1097/00010694-197003000-00003

Qi, R., Li, J., Lin, Z., Li, Z., Li, Y., Yang, X., Zhang, J., & Zhao, B. (2016). Temperature effects on soil organic carbon, soil labile organic carbon fractions, and soil enzyme activities under long-term fertilization regimes. *Applied Soil Ecology*, *102*, 36–45. https://doi.org/10.1016/j.apsoil.2016.02.004

Rao, S. E., Ray, L., Khan, T., & Ravi, G. (2022). Thermal conductivity, density and porosity of sedimentary and metamorphic rocks from the Lower and Higher Himalaya, Western Himalaya, India. *Geophysical Journal International*, *231*(1), 459–473. https://doi.org/10.1093/gji/ggac176

Raoof, A., & Hassanizadeh, S. M. (2012). A new formulation for pore-network modeling of two-phase flow. *Water Resources Research*, *48*(1), W01514. https://doi.org/10.1029/2010WR010180

Rostami, A., Habibagahi, G., Ajdari, M., & Nikooee, E. (2015). Pore network investigation on hysteresis phenomena and influence of stress state on the SWRC. *International Journal of Geomechanics*, *15*(5), 04014072. https://doi.org/10.1061/(ASCE)GM.1943-5622.0000315

Sanuade, O. A., Hassan, A. M., Akanji, A. O., Olaojo, A. A., Oladunjoye, M. A., & Abdulraheem, A. (2020). New empirical equation to estimate the soil moisture content based on thermal properties using machine learning techniques. *Arabian Journal of Geosciences*, *13*, 1–14. https://doi.org/10.1007/s12517-020-05375-x

Sedgewick, R. (1998). *Algorithms in C* (3rd ed.). Addison-Wesley.

Sepaskhah, A. R., & Boersma, L. (1979). Thermal conductivity of soils as a function of temperature and water content. *Soil Science Society of America Journal*, *43*, 439–444. https://doi.org/10.2136/sssaj1979.03615995004300030003x

Sharma, R. S., & Mohamed, M. H. (2003). An experimental investigation of LNAPL migration in an unsaturated/saturated sand. *Engineering Geology*, *70*(3–4), 305–313. https://doi.org/10.1016/S0013-7952(03)00098-X

Smits, K. M., Sakaki, T., Limsuwat, A., & Illangasekare, T. H. (2010). Thermal conductivity of sands under varying moisture and porosity in drainage–wetting cycles. *Vadose Zone Journal*, *9*(1), 172–180. https://doi.org/10.2136/vzj2009.0095

Somerton, W. H., El-Shaarani, A. H., & Mobarak, S. M. (1974, April 4–5). *High temperature behavior of rocks associated with geothermal type reservoirs* [Paper presentation]. SPE California Regional Meeting, San Francisco, CA, USA. https://doi.org/10.2118/4897-MS

Stauffer, F., & Dracos, T. (1984). Local infiltration into layered soil and response of the water table, experiment and simulation. *Frontiers in hydrology* (pp. 228–242). Water Resources Publication.

Stonestrom, D. A., & Rubin, J. (1989). Water content dependence of trapped air in two soils. *Water Resources Research*, *25*(9), 1947–1958. https://doi.org/10.1029/WR025i009p01947

Tang, A. M., Cui, Y. J., & Le, T. T. (2008). A study on the thermal conductivity of compacted bentonites. *Applied Clay Science*, *41*(3–4), 181–189. https://doi.org/10.1016/j.clay.2007.11.001

Tarnawski, V. R., & Leong, W. H. (2000). Thermal conductivity of soils at very low moisture content and moderate temperatures. *Transport in Porous Media*, *41*(2), 137–147. https://doi.org/10.1023/A:1006738727206

Tarnawski, V. R., Wagner, B., Leong, W. H., McCombie, M., Coppa, P., & Bovesecchi, G. (2021). Soil thermal conductivity model by de Vries: Re-examination and validation analysis. *European Journal of Soil Science*, *72*(5), 1940–1953. https://doi.org/10.1111/ejss.13117

Usowicz, B., Lipiec, J., Usowicz, J. B., & Marczewski, W. (2013). Effects of aggregate size on soil thermal conductivity: Comparison of measured and model-predicted data. *International Journal of Heat and Mass Transfer*, *57*(2), 536–541. https://doi.org/10.1016/j.ijheatmasstransfer.2012.10.067

Vahedifard, F., AghaKouchak, A., & Robinson, J. D. (2015). Drought threatens California's levees. *Science*, *349*(6250), 799–799. https://doi.org/10.1126/science.349.6250.799-a

Van Genuchten, M. T. (1980). A closed-form equation for predicting the hydraulic conductivity of unsaturated soils. *Soil Science Society of America Journal*, *44*(5), 892–898. https://doi.org/10.2136/sssaj1980.03615995004400050002x

Vu, Q. H., Pereira, J. M., & Tang, A. M. (2023). Effect of clay content on the thermal conductivity of unfrozen and frozen sandy soils. *International Journal of Heat and Mass Transfer*, *206*, 123923. https://doi.org/10.1016/j.ijheatmasstransfer.2023.123923

Xu, Y., Zeng, Z., & Lv, H. (2019). Effect of temperature on thermal conductivity of lateritic clays over a wide temperature range. *International Journal of Heat and Mass Transfer*, *138*, 562–570. https://doi.org/10.1016/j.ijheatmasstransfer.2019.04.077

Xu, Y., Zeng, Z., & Lv, H. (2020). Comparative study on thermal properties of undisturbed and compacted lateritic soils subjected to drying and wetting. *Engineering Geology*, *277*, 105800. https://doi.org/10.1016/j.enggeo.2020.105800

Yao, J. (2014). *Measurement and modeling of thermal properties of coarse-grained soils* [Master's thesis, University of Wisconsin-Madison].

Yu, X., Zhang, N., Pradhan, A., & Puppala, A. J. (2016). Geothermal energy for bridge deck and pavement deicing—A brief review. *GeoChicago*, *2016*, 598–609.

Zhang, J., Hou, J., Zhang, H., Meng, C., Zhang, X., & Wei, C. (2019). Low soil temperature inhibits yield of rice under drip irrigation. *Journal of Soil Science and Plant Nutrition*, *19*, 228–236. https://doi.org/10.1007/s42729-019-0008-x

Zhao, Y., & Si, B. (2019). Thermal properties of sandy and peat soils under unfrozen and frozen conditions. *Soil and Tillage Research*, *189*, 64–72. https://doi.org/10.1016/j.still.2018.12.026

Zhou, Y., Yan, C., Tang, A. M., Duan, C., & Dong, S. (2019). Mesoscopic prediction on the effective thermal conductivity of unsaturated clayey soils with double porosity system. *International Journal of Heat and Mass Transfer*, *130*, 747–756. https://doi.org/10.1016/j.ijheatmasstransfer.2018.11.001

How to cite this article: Mirghafari, R., Helforoosh, A. H., Nikooee, E., Habibagahi, G., Raoof, A., & van Genuchten, M. T. (2024). Pore unit cell network modeling of the thermal conductivity dynamics in unsaturated sandy soils: Unveiling the role of spanning-wetting phase cluster. *Vadose Zone Journal*, *23*, e20350. https://doi.org/10.1002/vzj2.20350

APPENDIX A

To determine the thermal conductivity (λ) of each soil unit cell embracing a pore, the λ values of the solid, air, and water phases were combined. Given the unknown value of λ of different sand types, an approximate mean value for sandstones (λ_s = 4.23 W/m K as reported by Rao et al. [2022]) was used. The thermal conductivities of water and air at room temperature were taken as λ_w = 0.56 and λ_a = 0.026 W/m K, respectively.

According to Cosenza et al. (2003), a quadratic parallel expression is recommended for complex multiphase materials to link the effective thermal conductivity of a unit cell containing solid, air, and water phases to their respective bulk values, through their volume fractions (φ). This approach has later been validated against 3D numerical heat flow simulations, showing promising results (Fedaoui et al., 2016). In this approach, the λ values of the solid, air, and water phases in a unit cell are combined using the following quadratic parallel expression:

$$\lambda_{\text{unit cell}} = \left(\sum_{i=1}^{3} \varphi_i \left(\sqrt{\lambda_i} \right) \right)^2. \tag{A1}$$

In our study, to reduce computational costs of running the PUCNM and to directly use soil thermal properties, this formulation was applied to eight sand types across different saturation levels (0.1–1). We found that the values of λ (unit cell) at these saturation levels can be empirically related to λ_{dry} and λ_{sat} of the soils as follows (Figure A1):

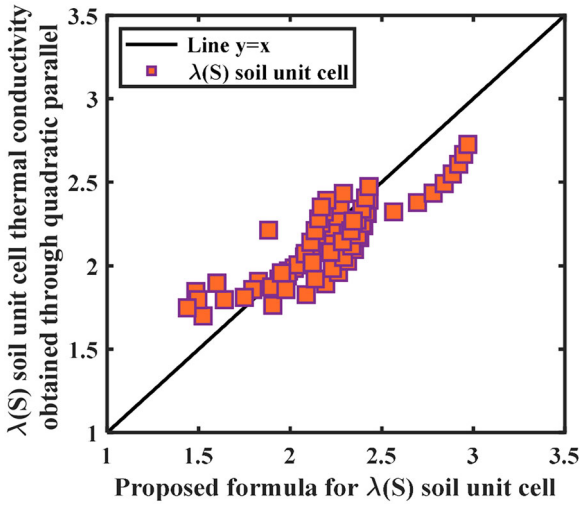

FIGURE A1 Comparison of effective unit cell thermal conductivities (λ) values (calculated using a quadratic parallel scheme) with values obtained from the proposed semi-empirical equation for eight sands and at different saturations (S = 0.1–1).

$$\lambda(S) = \left[\frac{\kappa S}{1 + (\kappa - 1)S} \right] (\lambda_{\text{sat}} - \lambda_{\text{dry}}) + \lambda_{\text{dry}}, \quad \kappa = 13. \tag{A2}$$

This equation is similar in form to the model suggested by Côté and Konrad (2005). However, in this study, we derived the equation based on a quadratic parallel conceptualization of solid, water, and air in a single pore unit cell. The equation connects local pore saturation (S) to the local conductivity (λ) of a pore unit cell, which could otherwise be obtained directly through quadratic parallel conceptualization.